

# Probing the Energy Landscape of the Membrane Protein Bacteriorhodopsin

Harald Janovjak,<sup>1</sup> Jens Struckmeier,<sup>3</sup>  
Maurice Hubain,<sup>1</sup> Alexej Kedrov,<sup>1</sup>  
Max Kessler,<sup>2</sup> and Daniel J. Müller<sup>1,\*</sup>

<sup>1</sup>BIOTEC

University of Technology Dresden  
01307 Dresden

<sup>2</sup>Lehrstuhl für Angewandte Physik  
Ludwig Maximilians Universität München  
80799 München

Germany

<sup>3</sup>Veeco Metrology

Digital Instruments

Santa Barbara, California 93117

## Summary

The folding and stability of transmembrane proteins is a fundamental and unsolved biological problem. Here, single bacteriorhodopsin molecules were mechanically unfolded from native purple membranes using atomic force microscopy and force spectroscopy. The energy landscape of individual transmembrane  $\alpha$  helices and polypeptide loops was mapped by monitoring the pulling speed dependence of the unfolding forces and applying Monte Carlo simulations. Single helices formed independently stable units stabilized by a single potential barrier. Mechanical unfolding of the helices was triggered by 3.9–7.7 Å extension, while natural unfolding rates were of the order of  $10^{-3} \text{ s}^{-1}$ . Besides acting as individually stable units, helices associated pairwise, establishing a collective potential barrier. The unfolding pathways of individual proteins reflect distinct pulling speed-dependent unfolding routes in their energy landscapes. These observations support the two-stage model of membrane protein folding in which  $\alpha$  helices insert into the membrane as stable units and then assemble into the functional protein.

## Introduction

Biological membranes are essential to all living organisms, as they provide selective permeability barriers and environments for a multitude of functional processes such as signal transduction, molecular transport, cell-to-cell communication, and cell adhesion (Lodish et al., 1999). Most functions of cellular membranes are carried out by integral membrane proteins which are therefore of fundamental biological interest and form major targets for drug development. However, the steadily increasing number of known gene sequences coding for membrane proteins contrasts sharply with our lacking knowledge of their functional three-dimensional structures as well as of their biosynthesis and stability within the lipid bilayer (Booth et al., 2001).

Membrane proteins acquire their unique functions

through the specific folding of their polypeptide in the anisotropic environment of the lipid bilayer (Haltia and Freire, 1995; Popot and Engelman, 2000; White and Wimley, 1999). In a so-called two-stage model, the sequential folding of  $\alpha$ -helical transmembrane proteins was described based on experimental results revealed from bacteriorhodopsin (BR) (Popot et al., 1987), which has now been confirmed on human aquaporin-1 and on the sodium-proton antiporter NhaA from *E. coli* (A. Kedrov, submitted; Möller et al., 2003). First, transmembrane helices form independently stable fragments which then assemble into the functional protein. Thus, it is suggested that the helices act comparably to domains in soluble proteins. Together with their connecting loops, the helices then assume a free energy minimum by the characteristic tertiary structure. Force spectroscopy data generated by mechanical unfolding of membrane proteins suggest that pairwise association of transmembrane helices drives them into a conformation of comparable stability to single transmembrane helices (A. Kedrov, submitted; Müller et al., 2002). This experimental finding is in agreement with the model given two decades ago that pairwise association builds a common structural motif in membrane protein folding and secretion (Engelman and Steitz, 1981).

The stability or resistance to unfolding of proteins is usually investigated by thermal or chemical denaturation in ensemble measurements. However, such bulk experimental methods only probe the average behavior of a large number of molecules and thus cannot resolve simultaneously occurring multiple (un)folding pathways and nonaccumulative intermediate folding states. Perceptions of protein (un)folding such as described by multidimensional landscapes or folding funnels can be seen as a result of the complexity of inter- and intramolecular interactions (Radford, 2000). Different (un)folding pathways may be populated in a manner dependent on small alterations of the physiological environment requiring novel investigative approaches (other than ensemble measurements) to observe coexisting minor and major pathways.

Experiments using the atomic force microscope (AFM) (Binnig et al., 1986) and similarly other force probe methods (Leckband and Israelachvili, 2001) provide novel techniques to reveal detailed insights into the molecular interactions determining the (un)folding of proteins. In these experiments, an external force applied to single proteins leads to sequential unfolding of their three-dimensional structure. Using this method in an assay will allow the screening of physiologically relevant parameters such as pH, electrolyte concentration, temperature, and other factors that modulate inter- and intramolecular interactions of the protein. In single-molecule force spectroscopy experiments using the AFM, a microfabricated cantilever detects molecular forces down to a few pN. A single molecule is tethered between the tip of the cantilever and a supporting surface while the tip-surface separation is continuously increased using a piezoelectric actuator. Recording the force against

\*Correspondence: mueller@mpi-cbg.de

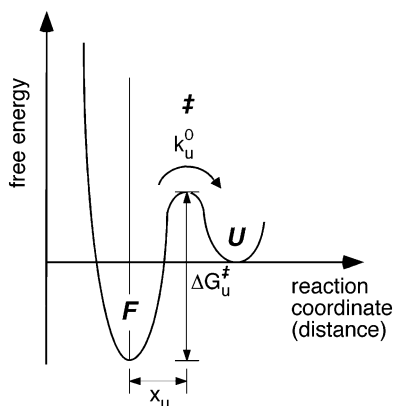


Figure 1. Two-State Model for the Interpretation of Mechanical Unfolding Experiments

A simple two-state potential exhibiting a single sharp potential barrier separating the folded low-energy state ( $F$ ) from the unfolded state ( $U$ ) can be applied to describe the mechanical unfolding experiments. Here the unfolding of single secondary structure elements of the membrane protein BR is interpreted using this model. The activation energy for unfolding is given by  $\Delta G_u^\ddagger$ , while  $x_u$  (the width of the potential barrier) is the distance along the reaction coordinate from the folded state to the transition state ( $\ddagger$ ) and the natural (thermal) transition rate is denoted  $k_u^0$ . DFS experiments allow determining the width of the potential barrier and the unfolding rate by monitoring the unfolding forces as a function of pulling speed.

tip-surface separation yields a force-extension curve characteristic for the particular molecule. In initial experiments, Rief and coworkers applied single-molecule force spectroscopy to the muscle protein titin which consists of repeats of globular immunoglobulin and tennascin domains (Rief et al., 1997). The continuous extension of the protein resulted in the subsequent unfolding of the globular domains while the forces necessary for unfolding of each domain are deduced from the force curve.

It was recently shown that dynamic force spectroscopy (DFS) experiments provide further insights into the energy landscape underlying the mechanical properties of single proteins and receptor ligand pairs. In DFS, single-molecule force spectroscopy AFM is extended to measure unfolding or unbinding forces at various pulling speeds. Monitoring the most probable rupture force as a function of the pulling speed allows resolving the width of potential barriers crossed during the unfolding process (Figure 1). Additionally, the natural transition rates over these barriers can be determined. Using this approach, the binding properties of individual ligand-receptor pairs (Merkel et al., 1999) and the unfolding behavior of globular proteins such as immunoglobulin were previously investigated (Carrion-Vazquez et al., 1999; Merkel et al., 1999; Williams et al., 2003). In case of immunoglobulin 27 (Ig 27) it was shown that a 3.3 Å extension triggers unfolding from an intermediate state (Carrion-Vazquez et al., 1999; Williams et al., 2003). Merkel and coworkers demonstrated that during unbinding of biotin from (strept)avidin several potential barriers are crossed and their positions along the separation distance could be localized (Merkel et al., 1999).

Here we apply DFS to probe the energy landscape of the integral membrane protein BR. To this end, single

proteins were unfolded from native purple membranes of *Halobacterium salinarum* at seven different pulling speeds in the range of 10 nm/s to 5.23  $\mu\text{m/s}$ . We have previously shown that the combination of single-molecule AFM imaging and force spectroscopy can be applied to unfold individual membrane proteins and determine the stability of their secondary structure elements (Möller et al., 2003; Müller et al., 2002; Oesterhelt et al., 2000). In contrast to most unfolding experiments on globular proteins, the membrane protein BR unfolds stepwise yielding surprisingly detailed insights into inter- and intramolecular interactions (Janovjak et al., 2003; Müller et al., 2002). In subsequent experiments, unfolding barriers stabilizing individual secondary structure elements of BR (such as transmembrane  $\alpha$  helices and polypeptide loops) were localized and the influence of external physiologically relevant parameters on these barriers was characterized (Janovjak et al., 2003; Müller et al., 2002). The DFS experiments performed in this work provided new detailed insights into potential barriers established by secondary structure elements. While single helices were found to be stabilized by a single potential barrier, they also associated pairwise, thereby establishing a different collective potential barrier. Mechanical unfolding of these structures was triggered by extension of a few angstroms, whereas natural unfolding rates were of the order of  $10^{-3} \text{ s}^{-1}$ .

The light-driven proton pump BR was chosen as model system for this study because it represents one of the most extensively studied membrane proteins. Its structural analysis has revealed the photoactive retinal embedded in seven closely packed transmembrane  $\alpha$  helices (Belrhali et al., 1999; Essen et al., 1998; Grigorieff et al., 1996; Luecke et al., 1999; Mitsuoka et al., 1999), a common structural motif among a large class of related G protein coupled receptors (Baldwin, 1993; Helmreich and Hofmann, 1996; Kolbe et al., 2000; Palczewski et al., 2000; Royant et al., 2001). Hydrophilic polypeptide loops link the seven membrane embedded hydrophobic BR helices lettered A through G, to which the C-terminal end is connected. With increasing knowledge of its structural and functional properties, BR has become a paradigm for  $\alpha$ -helical membrane proteins in general and for ion transporters in particular (Lanyi, 1999; Subramaniam, 1999).

## Results

Each superimposition shown in Figures 2A–2E is composed of  $\sim 15$  force curves, each recorded by unfolding a single BR molecule at the indicated pulling speed. It was previously shown that secondary structure elements of single BR molecules sequentially unfold when an external force is applied to the C terminus of the protein. Extension of the already unfolded elements then results in a characteristic pattern in the force spectrum (Figure 3). Apparently, the pulling speed did not change the unfolding pattern of BR and the individual force peaks remained at their positions (Figures 2A–2E). However, it is evident that the height of the force peaks and thus the average forces required to unfold parts of the protein increased with increasing pulling speed. By correlation to the three-dimensional structure of BR, we

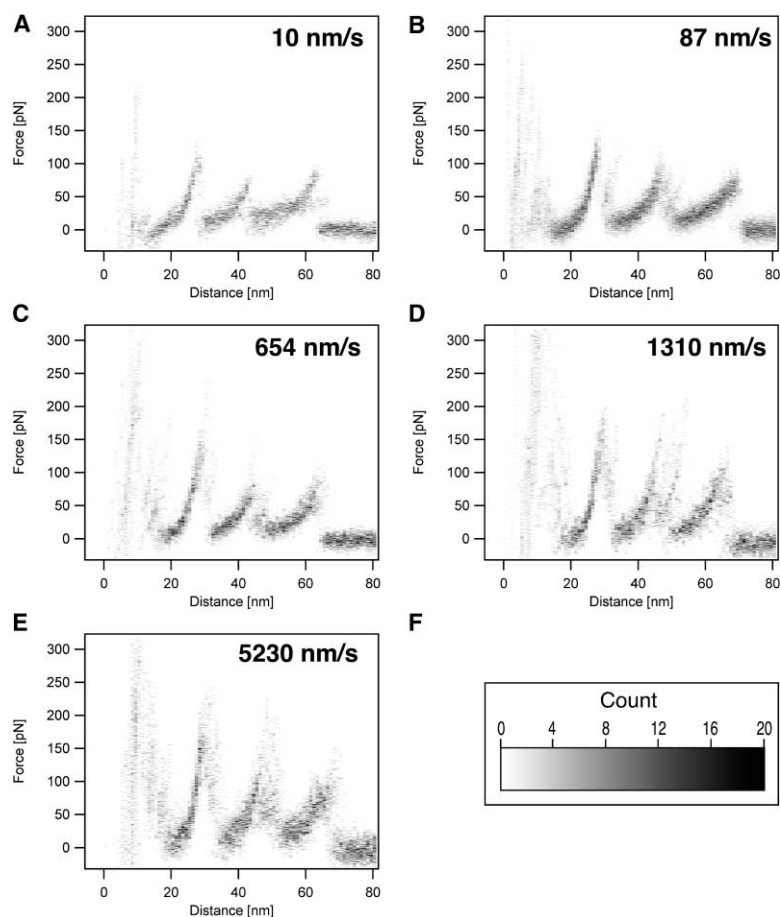


Figure 2. Superimpositions of BR Force Curves Recorded at Different Pulling Velocities

(A)–(E) show superimpositions of around 15 force versus distance traces each recorded on a single BR molecule at the pulling speed indicated (10 nm/s [A], 87 nm/s [B], 654 nm/s [C], 1310 nm/s [D], and 5230 nm/s [E]). As observed from the superimpositions, the unfolding forces (height of the peaks) increase with the pulling speed. The gray shading of the superimpositions was achieved by applying a grid subdividing each force curve into 1 pN by 1 nm big boxes and counting the number of data points in each box (a two-dimensional histogram). The scale in (F) shows that 20 data points will color individual boxes black (normalized to 10 curves with 2048 data points).

recently assigned the peaks in the force spectra to the unfolding of individual secondary structure elements such as transmembrane  $\alpha$  helices or polypeptide loops (Müller et al., 2002) (Figure 3).

Figure 4 shows the unfolding forces of secondary structure elements as a function of the logarithm of the pulling velocity, what is referred to as a dynamic force spectrum. The dynamic force spectrum for pairwise unfolding of two transmembrane helices is shown in Figure 4A, while those of single secondary structure elements are given in Figures 4B–4F. For all unfolding events, a single linear regime was observed in the dynamic force spectrum.

Among the different methods to analyze dynamic force spectra data we have chosen Monte Carlo (MC) simulations (Rief et al., 1998) as they take the (changing) length of the flexible polypeptide linker between the cantilever and membrane surface into account. MC simulations allow us to obtain the width ( $x_u$ ) and the natural unfolding rate ( $k_u^0$ ) of the potential barrier(s) crossed during an unfolding or unbinding process. This is achieved by systematically varying the two parameters of the MC simulation ( $x_u$  and  $k_u^0$ ) until the simulated forces and the measured forces are in best agreement. The goodness of the simulation was assessed by a chi-square comparison (see Experimental Procedures). The solid and dashed lines in Figure 4 represent the simulated forces as determined by the MC simulation with the minimal chi-square deviation from the measured data. The width

of the potential barrier and the natural unfolding rate used in these simulations are summarized in Table 1. For individual transmembrane helices we observed potential barriers' widths from 3.9 to 7.7 Å and spontaneous unfolding rates from  $1.8 \times 10^{-6}$  to  $1.7 \times 10^{-2}$  molecules per second. Pairwise unfolding of two helices and unfolding of the bc loop was characterized by potential barrier widths and unfolding rates in the same range of magnitude (3.2–6.8 Å for  $x_u$  and  $3.4 \times 10^{-5}$  to  $1.0 \times 10^{-2}$  for  $k_u^0$ ).

The above analysis showed that each individual structural element exhibited a free energy minimum, thereby establishing an internal potential barrier against mechanical unfolding. Although the transmembrane helices were sufficiently stable to unfold individually, they, at the same time, exhibited a distinct probability to unfold pairwise (Müller et al., 2002). Figure 5 shows that these unfolding probabilities were highly dependent on the pulling speed. While the unfolding probability of single transmembrane helices (dashed lines) increased with the pulling speed that of pairwise unfolding (solid lines) decreased.

## Discussion

### Force Spectroscopy of Individual Membrane Proteins

Single-molecule force spectroscopy experiments on membrane proteins such as BR, human aquaporin-1,

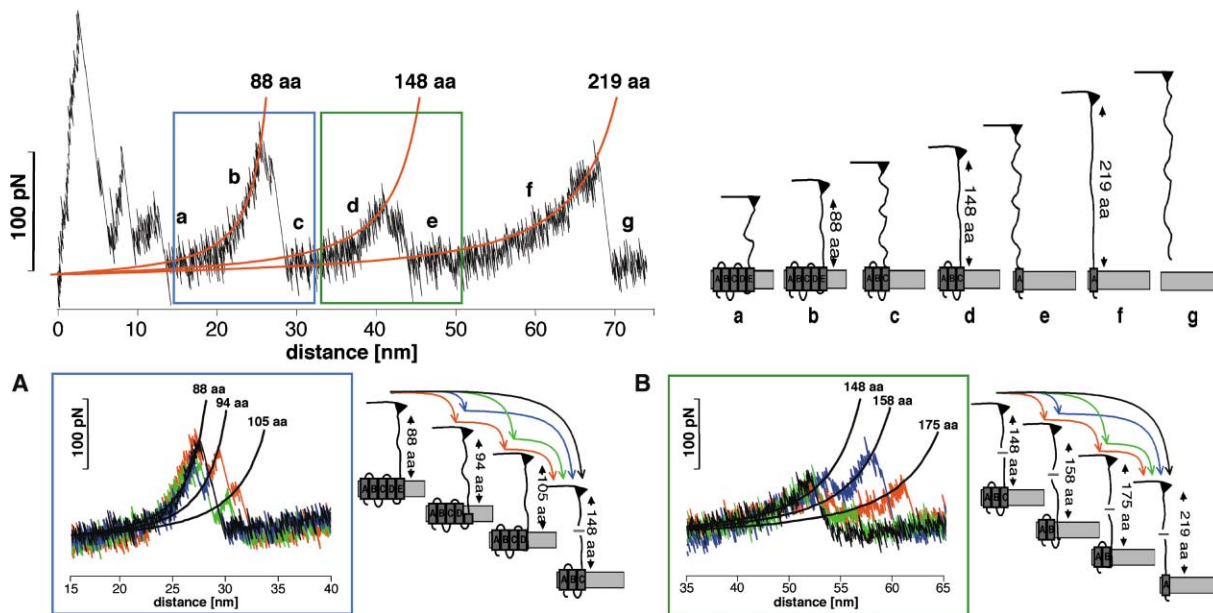


Figure 3. Unfolding Pathways of BR

Top, pairwise unfolding pathway of transmembrane  $\alpha$  helices. The experimental curve to the left shows a representative unfolding spectrum of a single BR, while the schematic unfolding pathway is sketched on the right. The worm-like chain model was applied to derive the length of the unfolded elements based on their force-extension pattern (solid lines). These lengths were then used to reconstruct the corresponding unfolding pathway (Müller et al., 2002). The first force peaks detected at tip-sample separations below 15 nm indicate the unfolding of transmembrane  $\alpha$  helices F and G. However, nonspecific interactions between the purple membrane surface and AFM tip are frequently observed in this part of the force spectrum and make a detailed analysis of these peaks difficult. After unfolding these elements, 88 aa are tethered between the tip and the surface (a). Separating the tip further from the surface stretches the polypeptide (b), thereby exerting force to helix E and D. At a certain critical load, the mechanical stability of helices E and D is overcome and they unfold together with loop DE. As the number of amino acids linking the tip and the surface is now increased to 148, the cantilever relaxes (c). In a next step, the 148 aa are extended thereby pulling on helix C (d). After unfolding helices B and C and loop BC in a single step, the molecular bridge is lengthened to 219 aa (e). By further separating tip and purple membrane, helix A unfolds (f) and the polypeptide is completely extracted from the membrane (g).

(A and B) Examples showing the unfolding of individual secondary structure elements. (A) Occasionally the first unfolding peak at 88 aa shows two shoulder peaks, which indicate the stepwise unfolding of the helical pair. If both shoulders occur, the peak at 88 aa indicates the unfolding of helix E, that at 94 aa of loop DE, and the peak at 105 aa corresponds to the unfolding of helix D. (B) The shoulder peaks of the second peak indicate the stepwise unfolding of helices C and B and loop BC. The peak at 148 aa indicates the unfolding of helix C, that at 158 aa of the loop BC, and the peak at 175 aa represents unfolding of helix B. The arrows indicate the observed unfolding pathways. In certain pathways (black arrows), a pair of two transmembrane helices and their connecting loop unfolded in a single step. In other unfolding pathways (colored arrows), these structural elements unfolded in several intermediate steps. We focused our analysis on the unfolding of single secondary structure elements, although in small number of events loops also unfolded together with helices.

and the bacterial sodium-proton antiporter NhaA recently yielded surprisingly detailed insights into their inter- and intramolecular interactions (A. Kedrov, submitted; Möller et al., 2003; Müller et al., 2002). To this end, one of the termini of the protein is attached to the tip of the AFM cantilever either by a covalent bond or more commonly by nonspecific attachment. Attachment of multiple sites of the terminus, polypeptide loops connecting the helices or intramembranous parts of the protein is largely excluded by limiting the analysis to force traces that show the length of a fully unfolded molecule (see Experimental Procedures). The protein is then mechanically unfolded using the cantilever as a force transducer applying an external force. Interactions that stabilize individual structural elements such as transmembrane  $\alpha$  helices and polypeptide loops were detected in terms of unfolding forces and different unfolding pathways (Müller et al., 2002). In this study, we investigated the speed dependence of the unfolding

forces to probe the energy landscape and the stability of single secondary structure elements.

#### Unfolding Forces Depend on the Pulling Speed

As first shown in Bell's seminal work and later in a more elaborate description by Evans and Ritchie, the escape over a potential barrier under a constant force ramp occurs within a time range determined by the applied force rate (Bell, 1978; Evans and Ritchie, 1997; Evans, 1999). At zero applied force, the spontaneous unfolding rate  $k_u^0$  (Figure 1) determines the time required to cross the barrier. Fast pulling speeds will result in low lifetimes, while low pulling speeds will render the bonds weak but lifetimes long. The unfolding force is thus governed by the pulling velocity and the width of the potential barrier  $x_u$  (the distance from the folded state to the transition state along the separation distance as the reaction coordinate) as well as the natural transition rate  $k_u^0$  (Figure

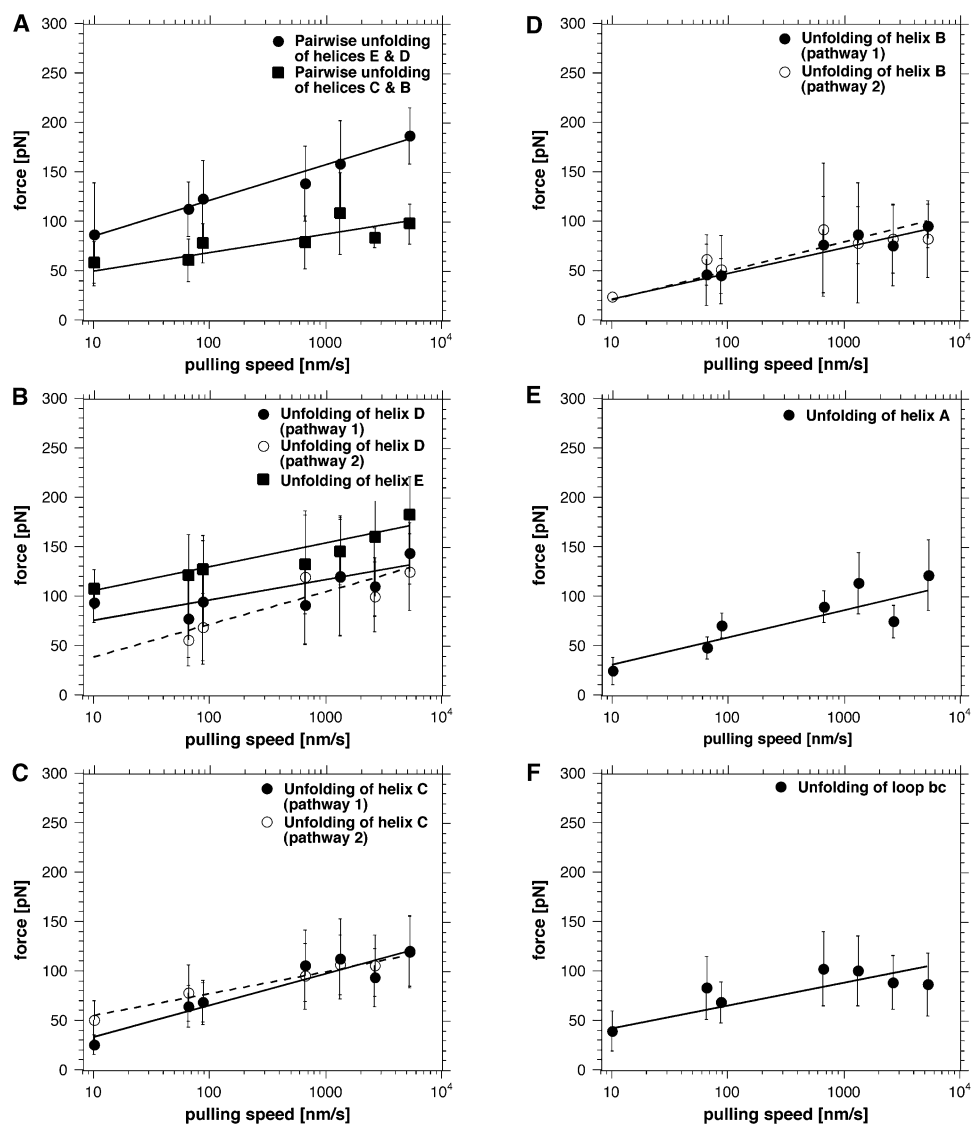


Figure 4. Unfolding Forces as a Function of Pulling Speed

For single and groups of secondary structure elements, the unfolding force increased with the pulling speed. A logarithmic dependence of the force on the pulling speed was clearly resolved. This indicated that a single sharp potential barrier as shown in Figure 1 was to be crossed to unfold the structural elements. Force versus  $\ln(\text{speed})$  plots for the pairwise unfolding of helices are shown in (A) and for single secondary structure elements (i.e., transmembrane  $\alpha$  helices and polypeptide loops) in (B)–(F). Solid and dashed lines represent Monte Carlo simulations (see Experimental Procedures) used to analyze the experimental data given by filled (in case of solid lines) and open symbols (in case of dashed lines). As unfolding of helices D, C, and B occurred in two different unfolding pathways (1 and 2), two data sets were obtained and analyzed independently. Although in both pathways these helices unfolded individually, other helices unfolded together with extracellular loops, and therefore the events were analyzed separately (Müller et al., 2002).

1) can be explored when pulling at different speeds (Evans and Ritchie, 1997; Evans, 1999).

#### Secondary Structure Elements of BR Establish Single Potential Barriers

The linear regime in force versus logarithm of the pulling speeds plots (Figure 4) suggests that a single sharp potential barrier such as shown in Figure 1, must be overcome (Evans and Ritchie, 1997; Evans, 1999). Thus, the potential landscape of mechanical unfolding can

be approximated by a two-state model. In this simple model, the low-energy folded state ( $F$ ) is separated from the unfolded state ( $U$ ) by the energy barrier located at the transition state ( $\ddagger$ ). Extension of the folded state by the width of the potential barrier ( $x_u$ ) triggers the unfolding process, and therefore  $x_u$  describes the position of the transition state along the reaction coordinate (separation). To obtain  $x_u$  from the data shown in Figure 4, we applied MC simulations (Rief et al., 1998). For individual transmembrane helices we observed  $x_u$  rang-

Table 1. Parameters Describing the Potential Barriers that Stabilize Secondary Structure Elements of BR against Mechanical Unfolding

Secondary Structure Element	Width of Potential ( $x_u$ [Å])	Natural Unfolding Rate ( $k_u^0$ [ $s^{-1}$ ])
Pairs of helices (Figure 4A)		
Helices E and D	3.2	$1.0 \times 10^{-2}$
Helices B and C	8.6	$3.4 \times 10^{-5}$
Individual helices (Figures 4B–4E)		
Helix E <sup>a</sup>	4.6	$1.1 \times 10^{-4}$
Helix D <sup>b</sup>	4.0 / 7.7	$5.6 \times 10^{-2}$ / $1.5 \times 10^{-6}$
Helix C <sup>b</sup>	4.9 / 3.9	$6.0 \times 10^{-3}$ / $5.6 \times 10^{-2}$
Helix B <sup>b</sup>	5.7 / 5.4	$1.7 \times 10^{-2}$ / $3.1 \times 10^{-2}$
Helix A	6.8	$1.8 \times 10^{-4}$
Individual loop (Figure 4F)		
Loop bc	5.8	$3 \times 10^{-3}$

The widths of the potential barrier and the natural unfolding rate of single and groups of secondary structure elements were determined by monitoring the unfolding force of each element as a function of the pulling speed.

<sup>a</sup>Including the 3 aa long loop ed.

<sup>b</sup>These elements unfold in two different unfolding pathways. Therefore, two values were obtained for  $x_u$  and  $k_u^0$ .

ing from 3.9 to 7.7 Å and for pairwise unfolding of transmembrane helices 3.2 and 8.6 Å (Table 1).

#### Extraction or Unfolding of Transmembrane Helices?

When extracting a biotinylated C18-lipid from stearyl-oleoyl phosphatidylcholine (SOPC) bilayers, Evans and Ludwig found that two potential barriers had to be crossed at 7 and 12 Å respectively (Evans and Ludwig, 2000). In agreement with the idea that lipid molecules are simply extracted from the membrane without a large degree of conformational change and consistent with the concept of hydrophobic interaction, the outer barrier is of comparable magnitude to half the bilayer membrane and the inner barrier correlates to the position of the unsaturated bond in the oleoyl chain (Evans and Ludwig, 2000). As one would expect, the position of the transition state during unfolding of a transmembrane helix is in apparent contrast to the ones observed during the extraction of lipid molecules from a membrane bilayer. The values observed here are much smaller than half the thickness of the purple membrane (which would correspond to about 30 Å) and thus suggest that breakage of inter- or intramolecular bonds stabilizing the structure starts the unfolding process. This initial step would then be followed by cooperative unfolding or “un-zipping” of the helical structures, in agreement with a

recently suggested model in which transmembrane helices unfold within the membrane rather than being first displaced from the hydrophobic membrane core (Janovjak et al., 2003). Molecular dynamics simulations will provide further insights into the details of the unfolding process including the exact sequence of events associated with the unzipping of individual helices. Complementary information about the interactions that stabilize single BRs can then also be obtained from the study of protein fragments (Hunt et al., 1997; Marti, 1998).

#### Stability of Individual Secondary Structure Elements

The MC simulations performed allow determination of the natural (zero applied force) transitions rate over the potential barriers. We found spontaneous unfolding rates in the range from  $1.5 \times 10^{-6}$  to  $1.7 \times 10^{-2} s^{-1}$  for single transmembrane helices and  $3.4 \times 10^{-5}$  to  $1.0 \times 10^{-2} s^{-1}$  for pairs of helices (Table 1). These values are of comparable magnitude to small globular proteins like barnase ( $k_u^0 = 2.3 \times 10^{-5} s^{-1}$ ) (Best et al., 2001) and Ig 27 ( $k_u^0 = 1.2 \times 10^{-4} s^{-1}$ ) (Carrion-Vazquez et al., 1999; Williams et al., 2003). This suggests that individual transmembrane helices which are considered important folding intermediates exhibit sufficient stability to form stable fragments prior to their assembly during the fast folding process (Allen et al., 2001).

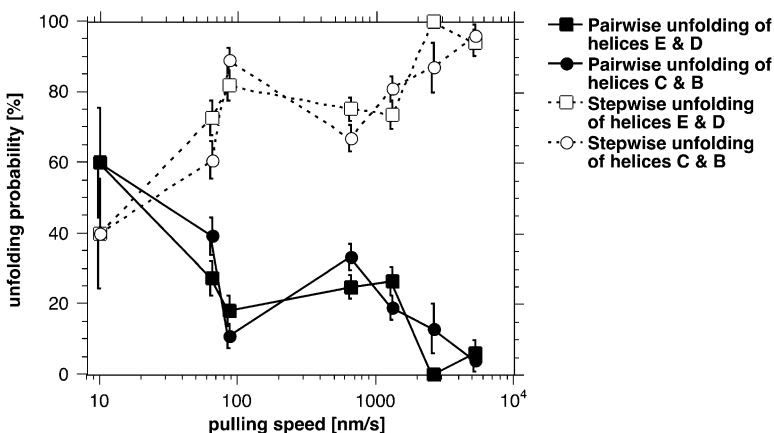


Figure 5. Unfolding Pathways Depend on Pulling Speed

Individual BR molecules exhibited distinct probabilities to follow different unfolding pathways when unfolded by mechanically pulling on the C terminus. Although single helices were sufficiently stable to unfold in individual steps (dashed lines), they exhibited a certain probability to unfold pairwise (solid lines). We found that changing the pulling speed affected these unfolding probabilities. As a result, the probability of unfolding single secondary structure elements increased with the pulling speed. This suggests that in the absence of a pulling force (smallest pulling speeds) two transmembrane helices would preferentially show a pairwise behavior (Figure 6).

### Unfolding Pathways of Individual BRs

It was previously shown that individual BR molecules follow well-defined unfolding pathways (Müller et al., 2002). These pathways differ as to whether secondary structure elements unfold individually or as grouped structures as observed for pairwise unfolding of transmembrane helices. Each of these pathways exhibits a distinct probability to be chosen. These probabilities can be altered by varying the physiological environment as well as by structural modifications of the protein (Janovjak et al., 2003; Müller et al., 2002). However, it could not be answered unambiguously whether changes in the probabilities to follow certain unfolding pathways reflected different unfolding trajectories in the potential landscape of the protein rather than different amounts of energy stored in the cantilever (Heymann and Grubmüller, 2000; Janovjak et al., 2003).

Our data clearly shows (Table 1) that the location of the transition state for certain unfolding events was different if they occurred in different unfolding pathways. For example, unfolding of the single helix E occurred at the same position in the force spectrum as pairwise unfolding of helices E and D (as the force is in both cases applied to helix E). However, in case of individual extraction of helix E an extension of 4.6 Å triggered unfolding, while in case of the pairwise unfolding of helices D and E the polypeptide had to be extended only 3.2 Å (Table 1). This indicates that two distinct unfolding routes along two different transition states were taken. This effect was also observed for the pairwise and stepwise unfolding of helices B and C.

### Rate Dependency of the Unfolding Pathways

The above observation is in agreement with the DFS data showing that the probabilities of the unfolding pathways depend on the pulling speed (Figure 5). By increasing the pulling speed, unfolding of individual transmembrane helices clearly dominated over pairwise unfolding. This indicates that the applied force tilted the potential barrier in such a way that the unfolding barrier for single transmembrane helices elements was lowered more than that for pairwise unfolding.

Pairwise association of transmembrane helices was suggested to play an important role in membrane protein stability and folding (Engelman and Steitz, 1981). Extrapolating the speed dependence of the pairwise unfolding pathways (Figure 5) to smaller pulling speeds (which at some point corresponds to zero unfolding force) suggests transmembrane helices almost exclusively unfold in a pairwise conformation. This indicates that under native conditions (zero applied force) the unfolding barrier for pairwise unfolding is smaller compared to the barrier for individual unfolding of the corresponding helices. Accordingly, the energy landscape can be approximated qualitatively such as shown in Figure 6. This behavior is also partly reflected in the natural transition rates revealed by the MC simulations (Table 1), where higher transition rates indicate the lower potential barrier. It should be noted however that the unfolding rates determined using MC simulations usually have a corresponding error of one order magnitude and thus cannot solely be used to justify our approximation of the potential landscape (Best et al., 2002).

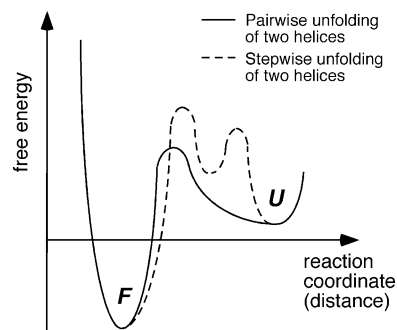


Figure 6. Potential Landscape as Revealed by Dynamic Force Spectroscopy

Two possible unfolding routes exist for pairs of transmembrane helices in BR. From the folded state (F), the two helices are either unfolded individually (dashed line) or pairwise (solid line) to the unfolded state (U). The shown approximation of the potential landscape at native conditions (zero force) was generated by extrapolating the speed-dependent unfolding probabilities to zero force (Figure 4). Since the experimental data showed that between two possible routes the pairwise unfolding was chosen more frequently, its potential barrier must be lower than for unfolding of individual helices.

### Conclusions

According to the currently accepted model, the biogenesis of multispinning membrane proteins occurs in two well-separated steps. First, transmembrane  $\alpha$  helices insert into the membrane as independently stable units before they assemble into the functional protein (Popot et al., 1987). Individual helical domains therefore are considered as important folding intermediates. Single-molecule force spectroscopy revealed that single helices form independently stable units and established potential barriers against mechanical unfolding. The experimental results revealed in this work show that individual helices are stabilized by one sharp potential barrier. It was also observed that helices associate pairwise forming a collective potential barrier. Both observations strongly support the two-stage model of membrane protein folding. The stability of single helices lies in the order of  $10^3$  s, which seems to be sufficient for assembly during the very fast folding process which takes place in milliseconds (Allen et al., 2001). We have shown that mechanical unfolding of single transmembrane helices is triggered by an extension of only  $\sim 4$  Å, which indicates that breakage of intramolecular interactions between or within secondary structure elements represents the starting point of a cooperative unfolding process.

### Experimental Procedures

#### Purple Membrane Preparation

Wild-type purple membrane was extracted from *H. salinarum* as described previously (Oesterhelt and Stoerkenius, 1974) and adsorbed onto freshly cleaved mica from buffer solution (300 mM KCl, 20 mM Tris, pH 7.8) (Müller et al., 1997). All buffer solutions were prepared with nanopure water and p.a. grade chemicals from Sigma/Merck.

#### Single-Molecule Force Spectroscopy

The AFM optimized for force spectroscopy (Multimode PicoForce, Nanoscope IIIa; Veeco Metrology, Santa Barbara, CA) was equipped with a 50  $\mu$ m X-Y-piezo scanner with a closed-loop 20  $\mu$ m z axis. The

spring constants of the 100  $\mu\text{m}$  long silicon nitride AFM cantilevers (Olympus OTR4, Veeco Metrology; nominal spring constant  $\sim 0.08$  N/m) were calibrated in solution using thermal fluctuation analysis (H.J. Butt and M. Jaschke, 1995, Nonotechnology, abstract; Florin et al., 1995). To perform force spectroscopy experiments, we recorded AFM topographs of the cytoplasmic purple membrane surface in 150 mM KCl, 10 mM Tris, and pH 7.8 (Müller et al., 1995). The AFM stylus was then approached to the cytoplasmic membrane surface and kept in contact with the proteins for about 1 s while applying a force between 300 and 1000 pN. Stylus and protein surface were then separated at velocities in the range of 10 nm/s to 5.23  $\mu\text{m/s}$ . In about 15% of all retraction curves we detected one or more adhesive peaks.

#### Attachment of BR to the AFM Cantilever

In earlier work we developed two different strategies to attach the protein to the tip. We have shown that a thiol group of the cysteine residue in the G241C mutant binds with a likelihood of  $\sim 90\%$  to a gold-coated cantilever when the tip is brought into contact with the cytoplasmic purple membrane surface at forces below 200 pN (Oesterhelt et al., 2000). Although this procedure allows a highly defined attachment, it requires replacement of the AFM cantilever after a few experiments since the tip is covered with bound proteins. An alternative method, nonspecific attachment to a silicon nitride cantilever using higher contact forces was shown to provide equivalent results and allows a much higher throughput (Müller et al., 2002). Since this study is a systematic investigation, we chose the nonspecific attachment as described above.

#### Force Curve Analysis

A clear criterion is required to distinguish curves of BR molecules attached to the AFM tip with different regions of their polypeptide backbone. One suitable criterion is the overall length of the force curve, which reflects the tip-sample distance at which the last force peak occurs (Oesterhelt et al., 2000). It is evident that a molecule attached to the cantilever by one of its loops results in a force curve of smaller overall length than a molecule attached by one of its termini. We have previously shown that force extension curves exhibiting an overall length between 60 and 70 nm result from completely unfolded and extended BR molecules attached with their C terminus to the AFM tip (Müller et al., 2002; Oesterhelt et al., 2000). This selection of force traces also assures that the protein has been contacted at the free C terminus and not in the intramembraneous part of the protein. All force curves exhibiting these overall lengths were selected and aligned with computer software according to the adhesion peak, which occurred at a tip-to-purple membrane separation of  $\sim 25$  nm (Figure 2). The alignment also compensates for attachment at multiple and/or different sites of the C terminus. To assign events in the force spectra to secondary structure elements, we have used the recently published mechanical unfolding pathways of BR (Müller et al., 2002). As proposed in this study, every peak of the force curves was fitted using the wormlike chain (WLC) model with a persistence length of 4 Å and a monomer length of 3.6 Å (Rief et al., 1997). The number of extended amino acids (aa) at each peak was then calculated using the contour length obtained from the WLC fits. To compare the polypeptide length with the BR structure the atomic model of Mitsuoka et al. (Mitsuoka et al., 1999) was chosen. To derive the unfolding forces and probabilities of the individual elements, every event of each curve was analyzed. We analyzed 10 (10 nm/s), 84 (50 nm/s), 79 (87 nm/s), 165 (654 nm/s), 121 (1310 nm/s), 23 (2620 nm/s), and 51 (5230 nm/s) individual force traces at the indicated pulling speed.

#### Dynamic Force Spectroscopy and MC simulations

We found that the unfolding forces of single secondary structure elements show a logarithmic dependence on the pulling velocity (Figure 4). This indicates that a single sharp potential barrier (as the one shown in Figure 1) is crossed during the unfolding process. To obtain the width of the potential barrier ( $x_u$ ) and the natural off-rate ( $k_u^0$ ) from the DFS data we applied MC simulations (Rief et al., 1998). We performed simulations for pairs of  $x_u$  (ranging from 1 to 10 Å with 80 linear increments) and  $k_u^0$  (ranging from 1 to  $10^{-5}$  s $^{-1}$  with 20 logarithmic increments). For each pair of  $x_u$  and  $k_u^0$  the goodness

of the simulations was determined by calculating chi-square ( $\chi^2$ ) according to:

$$\chi^2(\chi_u, k_u^0) = \sum_{i=1}^N \left( \frac{f_{\text{exp}}(v_i) - f_{\text{sim}}(v_i; \chi_u, k_u^0)}{\sigma_i} \right)^2, \quad (1)$$

where  $f_{\text{exp}}$  is the measured forces,  $f_{\text{sim}}$  the forces determined by MC simulations at the same speed, and  $\sigma$  denotes the standard deviation of the measured forces (Best et al., 2002). The best pair of parameters was found by looking for minimal  $\chi^2$  (Best et al., 2002).

#### Acknowledgments

We would like to thank Matthias Rief, Kate Poole, and Tanuj Sapra for fruitful discussions. The Volkswagenstiftung, European Community, and State of Saxony supported this work.

Received: November 23, 2003

Revised: February 26, 2004

Accepted: March 2, 2004

Published: May 11, 2004

#### References

- Allen, S.J., Kim, J.M., Khorana, H.G., Lu, H., and Booth, P.J. (2001). Structure and function in bacteriorhodopsin: the effect of the interhelical loops on the protein folding kinetics. *J. Mol. Biol.* **308**, 423–435.
- Baldwin, J.M. (1993). The probable arrangement of the helices in G protein-coupled receptors. *EMBO J.* **12**, 1693–1703.
- Bell, G.I. (1978). Models for the specific adhesion of cells to cells. *Science* **200**, 618–627.
- Belrhali, H., Nollert, P., Royant, A., Menzel, C., Rosenbusch, J.P., Landau, E.M., and Pebay-Peyroula, E. (1999). Protein, lipid and water organization in bacteriorhodopsin crystals: a molecular view of the purple membrane at 1.9 Å resolution. *Struct. Fold. Des.* **7**, 909–917.
- Best, R.B., Li, B., Steward, A., Daggett, V., and Clarke, J. (2001). Can non-mechanical proteins withstand force? Stretching barnase by atomic force microscopy and molecular dynamics simulation. *Biophys. J.* **81**, 2344–2356.
- Best, R.B., Fowler, S.B., Toca-Herrera, J.L., and Clarke, J. (2002). A simple method for probing the mechanical unfolding pathway of proteins in detail. *Proc. Natl. Acad. Sci. USA* **99**, 12143–12148.
- Binnig, G., Quate, C.F., and Gerber, C. (1986). Atomic force microscope. *Phys. Rev. Lett.* **56**, 930–933.
- Booth, P.J., Templer, R.H., Curran, A.R., and Allen, S.J. (2001). Can we identify the forces that drive the folding of integral membrane proteins? *Biochem. Soc. Trans.* **29**, 408–413.
- Carrion-Vazquez, M., Oberhauser, A.F., Fowler, S.B., Marszalek, P.E., Broedel, S.E., Clarke, J., and Fernandez, J.M. (1999). Mechanical and chemical unfolding of a single protein: a comparison. *Proc. Natl. Acad. Sci. USA* **96**, 3694–3699.
- Engelman, D.M., and Steitz, T.A. (1981). The spontaneous insertion of proteins into and across membranes: the helical hairpin hypothesis. *Cell* **23**, 411–422.
- Essen, L., Siegert, R., Lehmann, W.D., and Oesterhelt, D. (1998). Lipid patches in membrane protein oligomers: crystal structure of the bacteriorhodopsin-lipid complex. *Proc. Natl. Acad. Sci. USA* **95**, 11673–11678.
- Evans, E.B. (1999). Looking inside molecular bonds at biological interfaces with dynamic force spectroscopy. *Biophys. Chem.* **82**, 83–97.
- Evans, E., and Ludwig, F. (2000). Dynamic strengths of molecular anchoring and material cohesion in fluid biomembranes. *J. Phys. Condens. Matter* **12**, A315–A320.
- Evans, E., and Ritchie, K. (1997). Dynamic strength of molecular adhesion bonds. *Biophys. J.* **72**, 1541–1555.
- Florin, E.L., Rief, M., Lehmann, H., Ludwig, M., Dornmair, C., Moy, V.T., and Gaub, H.E. (1995). Sensing specific molecular-interactions

- with the atomic force microscope. *Biosens. Bioelectron.* **10**, 895–901.
- Grigorieff, N., Ceska, T.A., Downing, K.H., Baldwin, J.M., and Henderson, R. (1996). Electron-crystallographic refinement of the structure of bacteriorhodopsin. *J. Mol. Biol.* **259**, 393–421.
- Haltia, T., and Freire, E. (1995). Forces and factors that contribute to the structural stability of membrane proteins. *Biochim. Biophys. Acta* **1241**, 295–322.
- Helmreich, E.J., and Hofmann, K.P. (1996). Structure and function of proteins in G-protein-coupled signal transfer. *Biochim. Biophys. Acta* **1286**, 285–322.
- Heymann, B., and Grubmüller, H. (2000). Dynamic force spectroscopy of molecular adhesion bonds. *Phys. Rev. Lett.* **84**, 6126–6129.
- Hunt, J.F., Earnest, T.N., Bousche, O., Kalghatgi, K., Reilly, K., Horvath, C., Rothschild, K.J., and Engelman, D.M. (1997). A biophysical study of integral membrane protein folding. *Biochemistry* **36**, 15156–15176.
- Janovjak, H., Kessler, M., Oesterhelt, D., Gaub, H., and Muller, D.J. (2003). Unfolding pathways of native bacteriorhodopsin depend on temperature. *EMBO J.* **22**, 5220–5229.
- Kolbe, M., Besir, H., Essen, L.O., and Oesterhelt, D. (2000). Structure of the light-driven chloride pump halorhodopsin at 1.8 Å resolution. *Science* **288**, 1390–1396.
- Lanyi, J.K. (1999). Progress toward an explicit mechanistic model for the light-driven pump, bacteriorhodopsin. *FEBS Lett.* **464**, 103–107.
- Leckband, D., and Israelachvili, J. (2001). Intermolecular forces in biology. *Q. Rev. Biophys.* **34**, 105–267.
- Lodish, H., Berk, A., Zipursky, L.S., Matsudaira, P., Baltimore, D., and Darnell, J.E. (1999). *Molecular Cell Biology*, Fourth Edition (New York: W.H. Freeman and Company).
- Luecke, H., Schobert, B., Richter, H.T., Cartailler, J.P., and Lanyi, J.K. (1999). Structure of bacteriorhodopsin at 1.55 Å resolution. *J. Mol. Biol.* **291**, 899–911.
- Marti, T. (1998). Refolding of bacteriorhodopsin from expressed polypeptide fragments. *J. Biol. Chem.* **273**, 9312–9322.
- Merkel, R., Nassoy, P., Leung, A., Ritchie, K., and Evans, E. (1999). Energy landscapes of receptor-ligand bonds explored with dynamic force spectroscopy. *Nature* **397**, 50–53.
- Mitsuoka, K., Hirai, T., Murata, K., Miyazawa, A., Kidera, A., Kimura, Y., and Fujiyoshi, Y. (1999). The structure of bacteriorhodopsin at 3.0 Å resolution based on electron crystallography: implication of the charge distribution. *J. Mol. Biol.* **286**, 861–882.
- Möller, C., Fotiadis, D., Suda, K., Engel, A., Kessler, M., and Muller, D.J. (2003). Determining molecular forces that stabilize human aquaporin-1. *J. Struct. Biol.* **142**, 369–378.
- Müller, D.J., Schabert, F.A., Büldt, G., and Engel, A. (1995). Imaging purple membranes in aqueous solutions at sub-nanometer resolution by atomic force microscopy. *Biophys. J.* **68**, 1681–1686.
- Müller, D.J., Amrein, M., and Engel, A. (1997). Adsorption of biological molecules to a solid support for scanning probe microscopy. *J. Struct. Biol.* **119**, 172–188.
- Müller, D.J., Kessler, M., Oesterhelt, F., Möller, C., Oesterhelt, D., and Gaub, H. (2002). Stability of bacteriorhodopsin alpha-helices and loops analyzed by single-molecule force spectroscopy. *Biophys. J.* **83**, 3578–3588.
- Oesterhelt, D., and Stoekenius, W. (1974). Isolation of the cell membrane of *Halobacterium halobium* and its fractionation into red and purple membrane. *Methods Enzymol.* **31**, 667–678.
- Oesterhelt, F., Oesterhelt, D., Pfeiffer, M., Engel, A., Gaub, H.E., and Müller, D.J. (2000). Unfolding pathways of individual bacteriorhodopsins. *Science* **288**, 143–146.
- Palczewski, K., Kumasaka, T., Hori, T., Behnke, C.A., Motoshima, H., Fox, B.A., Le Trong, I., Teller, D.C., Okada, T., Stenkamp, R.E., et al. (2000). Crystal structure of rhodopsin: A G protein-coupled receptor. *Science* **289**, 739–745.
- Popot, J.L., and Engelman, D.M. (2000). Helical membrane protein folding, stability, and evolution. *Annu. Rev. Biochem.* **69**, 881–922.
- Popot, J.L., Gerchman, S.E., and Engelman, D.M. (1987). Refolding of bacteriorhodopsin in lipid bilayers. A thermodynamically controlled two-stage process. *J. Mol. Biol.* **198**, 655–676.
- Radford, S.E. (2000). Protein folding: progress made and promises ahead. *Trends Biochem. Sci.* **25**, 611–618.
- Rief, M., Gautel, M., Oesterhelt, F., Fernandez, J.M., and Gaub, H.E. (1997). Reversible unfolding of individual titin immunoglobulin domains by AFM. *Science* **276**, 1109–1112.
- Rief, M., Fernandez, J.M., and Gaub, H.E. (1998). Elastically coupled two-level systems as a model for biopolymer extensibility. *Phys. Rev. Lett.* **81**, 4764–4767.
- Royant, A., Nollert, P., Edman, K., Neutze, R., Landau, E.M., Pebay-Peyroula, E., and Navarro, J. (2001). X-ray structure of sensory rhodopsin II at 2.1-Å resolution. *Proc. Natl. Acad. Sci. USA* **98**, 10131–10136.
- Subramaniam, S. (1999). The structure of bacteriorhodopsin: an emerging consensus. *Curr. Opin. Struct. Biol.* **9**, 462–468.
- White, S.H., and Wimley, W.C. (1999). Membrane protein folding and stability: physical principles. *Annu. Rev. Biophys. Biomol. Struct.* **28**, 319–365.
- Williams, P.M., Fowler, S.B., Best, R.B., Toca-Herrera, J.L., Scott, K.A., Steward, A., and Clarke, J. (2003). Hidden complexity in the mechanical properties of titin. *Nature* **422**, 446–449.